



UNIVERSITY OF LEEDS

This is a repository copy of *Subsurface structural interpretation by applying trishear algorithm: an example from the Lenghu5 fold-and-thrust belt, Qaidam Basin, Northern Tibetan Plateau*.

White Rose Research Online URL for this paper:  
<http://eprints.whiterose.ac.uk/116221/>

Version: Accepted Version

---

**Article:**

Pei, Y, Paton, DA, Wu, K et al. (1 more author) (2017) Subsurface structural interpretation by applying trishear algorithm: an example from the Lenghu5 fold-and-thrust belt, Qaidam Basin, Northern Tibetan Plateau. *Journal of Asian Earth Sciences*, 143. pp. 343-353. ISSN 1367-9120

<https://doi.org/10.1016/j.jseaes.2017.05.012>

---

© 2017 Elsevier Ltd. This manuscript version is made available under the CC-BY-NC-ND 4.0 license <http://creativecommons.org/licenses/by-nc-nd/4.0/>

**Reuse**

Items deposited in White Rose Research Online are protected by copyright, with all rights reserved unless indicated otherwise. They may be downloaded and/or printed for private study, or other acts as permitted by national copyright laws. The publisher or other rights holders may allow further reproduction and re-use of the full text version. This is indicated by the licence information on the White Rose Research Online record for the item.

**Takedown**

If you consider content in White Rose Research Online to be in breach of UK law, please notify us by emailing [eprints@whiterose.ac.uk](mailto:eprints@whiterose.ac.uk) including the URL of the record and the reason for the withdrawal request.



[eprints@whiterose.ac.uk](mailto:eprints@whiterose.ac.uk)  
<https://eprints.whiterose.ac.uk/>

## Accepted Manuscript

Full length article

Subsurface structural interpretation by applying trishear algorithm: an example from the Lenghu5 fold-and-thrust belt, Qaidam Basin, Northern Tibetan Plateau

Yangwen Pei, Douglas A. Paton, Kongyou Wu, Liujuan Xie

PII: S1367-9120(17)30228-6

DOI: <http://dx.doi.org/10.1016/j.jseaes.2017.05.012>

Reference: JAES 3077

To appear in: *Journal of Asian Earth Sciences*

Received Date: 12 October 2016

Revised Date: 4 May 2017

Accepted Date: 7 May 2017

Please cite this article as: Pei, Y., Paton, D.A., Wu, K., Xie, L., Subsurface structural interpretation by applying trishear algorithm: an example from the Lenghu5 fold-and-thrust belt, Qaidam Basin, Northern Tibetan Plateau, *Journal of Asian Earth Sciences* (2017), doi: <http://dx.doi.org/10.1016/j.jseaes.2017.05.012>

This is a PDF file of an unedited manuscript that has been accepted for publication. As a service to our customers we are providing this early version of the manuscript. The manuscript will undergo copyediting, typesetting, and review of the resulting proof before it is published in its final form. Please note that during the production process errors may be discovered which could affect the content, and all legal disclaimers that apply to the journal pertain.



**Subsurface structural interpretation by applying trishear algorithm: an example from the Lenghu5 fold-and-thrust belt, Qaidam Basin, Northern Tibetan Plateau**

Yangwen Pei<sup>a, c, \*</sup>, Douglas A. Paton<sup>b</sup>, Kongyou Wu<sup>a</sup>, Liujuan Xie<sup>a</sup>

<sup>a</sup> School of Geosciences, China University of Petroleum, Qingdao, 266580, China

<sup>b</sup> School of Earth & Environment, University of Leeds, Leeds, West Yorkshire, LS2 9JT, England

<sup>c</sup> Key Laboratory of Tectonics and Petroleum Resources (China University of Geosciences), Ministry of Education, Wuhan 430074, China

\* Corresponding author. Email: peiyangwen@upc.edu.cn.

**Abstract**

The application of trishear algorithm, in which deformation occurs in a triangle zone in front of a propagating fault tip, is often used to understand fault related folding. In comparison to kink-band methods, a key characteristic of trishear algorithm is that non-uniform deformation within the triangle zone allows the layer thickness and horizon length to change during deformation, which is commonly observed in natural structures. An example from the Lenghu5 fold-and-thrust belt (Qaidam Basin, northern Tibetan Plateau) is interpreted to help understand how to employ trishear forward modelling to improve the accuracy of seismic interpretation. High resolution fieldwork data, including high-angle dips, 'dragging structures', thinning hanging-wall and thickening footwall, are used to determine best-fit trishear model to explain the deformation happened to the Lenghu5 fold-and-thrust belt. We also consider the factors that increase the complexity of trishear models, including: (a) fault-dip changes and (b) pre-existing faults. We integrate fault dip change and pre-existing faults to predict subsurface structures that are apparently under seismic resolution.

The analogue analysis by trishear models indicates that the Lenghu5 fold-and-thrust belt is controlled by an upward-steepening reverse fault above a pre-existing opposite-thrusting fault in deeper subsurface. The validity of the trishear model is confirmed by the high accordance between the model and the high-resolution fieldwork. The validated trishear forward model provides geometric constraints to the faults and horizons in the seismic section, e.g., fault cutoffs and fault tip position, faults' intersecting relationship and horizon/fault cross-cutting relationship. The subsurface prediction using trishear algorithm can significantly increase the accuracy of seismic interpretation, particularly in seismic sections with low signal/noise ratio.

### **Keywords**

trishear algorithm, high-resolution fieldwork, structural complexity, geometric constraints, subsurface prediction

### **Introduction**

It has been extensively documented from outcrop and sub-surface studies that there is an intimate relationship between folding of sedimentary sequences and underlying faults, and a variety of different models are invoked, including fault-bend folding (Jamison, 1987; Medwedeff and Suppe, 1997; Suppe, 1983; Tavani et al., 2005), fault-propagation folding (Jamison, 1987; Mitra, 1990; Suppe and Medwedeff, 1990) and detachment folding (Dahlstrom, 1990; Jamison, 1987; Mitra, 2003; Poblet and McClay, 1996) to explain specific examples. Many of these models utilise a kink-band method (Fig. 1a, b) that maintains a constant layer thickness and line length, which results in uniform dips and homogeneous deformation of the fold limbs (Suppe, 1983; Suppe and Medwedeff, 1990).

However, there have been many examples that cannot be well illustrated by kink-band method, including both experimental analogue studies (e.g., Bose et al., 2009;

Ellis et al., 2004; McQuarrie, 2004; Miller and Mitra, 2011) and natural geological structures (e.g., Allmendinger, 1998; Cristallini and Allmendinger, 2001; Erslev, 1991; Erslev and Mayborn, 1997; Erslev and Rogers, 1993). For example, Fig. 2a shows a natural example of trishear algorithm, which is a simplified cross section of the Turner Valley anticline, Canadian Rocky Mountains (Allmendinger, 1998). The Turner Valley anticline is controlled by the underlying reverse fault. Against the reverse fault, 'dragging structures' are developed, with an anticline in the hanging-wall and a syncline in the footwall, respectively. The trishear algorithm, maintaining section area during deformation, provides an alternative approach for those examples (Fig. 2b). Trishear mechanism was initially proposed by (Erslev, 1991), with a precondition that the section area is kept constant during deformation, allowing non-uniform dip and inhomogeneous strain occurs within the folds/faults. Within the trishear model, the deformation is concentrated within a triangle zone in front of the propagating fault tip. The trishear algorithm is determined by multiple parameters, e.g., trishear p/s ratio (the fault propagation/slip ratio), trishear apical angle, fault dip, etc.

Despite these studies on trishear algorithm, little attention has been paid on the integration of high-resolution field data, which limits the application of the trishear mechanism in subsurface structural prediction, particularly the structural features that are under seismic resolution. In this paper, we focus on prediction of subsurface structural geometry by employing trishear forward modelling. An example from the Lenghu5 fold-and-thrust belt in the Qaidam Basin (Northern Tibetan Plateau) is interpreted using the trishear algorithm, with validation by high-resolution field data, which provides an effective workflow of applying trishear algorithm to complex natural structures.

## 1. Geological Settings

The Cenozoic Qaidam Basin, with an average elevation of 2.8 km, is one of the largest sedimentary basins in the northern Tibetan Plateau (Fig. 3a). The Qaidam Basin presents a triangular shape in plain view (Fig. 3b), bounded by the QilianShan-NanShan Thrust Belt to the northeast, the Altyn Tagh Strike-slip Fault to the northwest and the QimenTagh-EasternKunlun Belt to the southwest (e.g. Burchfiel et al., 1989; Cowgill et al., 2000; Cowgill et al., 2003; e.g. Jolivet et al., 2003; Meyer et al., 1998; Tapponnier et al., 1990; Yin et al., 2007; Yin et al., 2008a; Yin and Harrison, 2000). The stratigraphy of Qaidam Basin is divided into three main packages, which are metamorphic basement, late Palaeozoic-Mesozoic package and Cenozoic package (e.g., Cui et al., 1995; Deng et al., 1995; Gao et al., 1995; Xia et al., 2001).

In Fig. 3c, a cross section, through the central portion of Qaidam Basin, is constructed based on the published studies (e.g., Liu et al., 2009; Yin et al., 2008b; Zhou et al., 2006). The NE-SW section (see position in Fig. 3b), ~180 km long, covers majority of the Qaidam Basin to present both the primary and regional structural geometry. In this section, the Qaidam Basin develops different orders of structures. The first-order structure is a large-scale synclinorium composed of a series of tight anticlines and open synclines, with a wavelength of ~380 km (length of Fig. 3c section is half wavelength) and amplitude of ~16 km. The Qaidam Basin develops huge thick Cenozoic strata up to 16 km and locally thin Mesozoic strata. The central thickening of Cenozoic stratigraphic units suggests that the development of Qaidam Basin is controlled by NE-SW compression, which is derived from the uplift of Tibetan Plateau (e.g., Cheng et al., 2015; Cheng et al., 2017; Mao et al., 2016; Molnar and Tapponnier, 1975; Wang and Burchfiel, 2004; Wei et al., 2016; Wu

et al., 2014; Yin et al., 2008a; Yin et al., 2008b; Yin and Harrison, 2000; Yu et al., 2014; Zhou et al., 2006; Zhu et al., 2006). The second-order structures are regional scale folds and faults. The inversed normal faults in Mesozoic strata and thrust faults in Jurassic-Eocene strata, forming fault-bend folds and fault-propagation folds, indicate a complicated structural deformation in the Qaidam Basin. The Lenghu5 fold-and-thrust belt, our study area, is located in the north Qaidam Basin (see position in Fig. 3c).

## 2. Structural Geometry of the Lenghu5 Fold-and-thrust Belt

In order to understand the structural geometry of the Lenghu5 fold-and-thrust belt, a depth-converted seismic section is constructed, with length of ~18 km and depth of ~9 km (Fig. 4). This section is well constrained by the 'Lengke1' well and the regional stratigraphy (Fig. 4a). An upward-steepening reverse fault ( $F_1$ ) and an opposite-dipping thrust fault ( $F_2$ ) are picked up in this seismic section (Fig. 4b). The stratigraphy is composed of basement, Mesozoic strata ( $J_r$ ) and Cenozoic strata ( $E_{1+2}$ - $N_{2-2}$ ). The thicker unit  $J_r$  in the hanging-wall than the footwall, suggests that  $F_2$  was initially a normal fault and is inversed in a later compression. The units of  $E_{1+2}$ - $N_{2-1}$  keep constant thickness throughout the section, suggesting that these units are deposited before the later compression. The growth strata developed in unit  $N_{2-2}$  indicate that unit  $N_{2-2}$  is deposited simultaneously with the compression (Fig. 4c).

Therefore, the Lenghu5 fold-and-thrust belt experience an inversion from the initial Mesozoic extension to the later Cenozoic compression. The fault  $F_2$  was developed as a normal fault in the initial Mesozoic extension and transferred to be an inverted fault when it was subject to the later Cenozoic compression. However, the high angle  $F_2$  was apparently too steep for the hanging-wall to move upward continuously upon the fault plane. Therefore, a low angle thrust fault  $F_1$  was, therefore, developed in the

upper  $E_3$  unit to accommodate the compressional strain happened to the Lenghu5 fold-and-thrust belt. The interaction between  $F_1$  and  $F_2$  determines the resultant geometry of this structure.

However, the conventional structural restoration, using 'fault parallel flow' algorithm in 2D Move (Midland Valley), presents imbalance of the restored sections (Fig. 5).

For example, the unit  $E_3$  (the cyan layer) does not present constant thickness after the connection of the cutoffs A and A' by restoring the hanging-wall down the fault  $F_1$  ( $h_1$ ,  $h_2$  and  $h_3$  in Fig. 5b). Moreover, the intersecting relationship between the faults  $F_1$  and  $F_2$  is also unclear, because the tip of  $F_2$  cannot be accurately determined based on the poor quality of seismic reflection. This hinders our understanding in the detailed deformation happened to the Lenghu5 fold-and-thrust belt. Given the detailed structural features (e.g., high-angle dip variation and small folds that are under seismic resolution) are usually not resolvable in seismic reflection, a high-resolution fieldwork is therefore necessary to understand fault architecture and structural deformation of the Lenghu5 fold-and-thrust belt.

### 3. High-resolution Fieldwork

In the Lenghu5 fold-and-thrust belt, the topography is relatively flat (see the QuickBird image in Fig. 6). Because of arid weather and strong winds, there are very limited plants and the rocks are well exposed in surface. In the high-resolution QuickBird image (with spatial resolution of 1 m, derived from DigitalGlobal), layering of stratigraphy is well imaged with different colours that are determined by lithology. In the QuickBird image, coarse sandstones or conglomerates present grey or light brown colour, medium to fine sandstones present brown colour, whereas siltstones and mudstones present reddish brown colour. Being constrained by the satellite image, the detailed stratigraphy is recorded in a high-resolution fieldwork, including a

column HW for the hanging-wall and a column FW for the footwall (see the horizontal columns in top of Fig. 6). These two stratigraphic columns HW and FW present thickness of ~1200 m and ~650 m, respectively. The stratigraphic columns are horizontally aligned with a high-resolution satellite image to assist the profile construction (see position of this section in Fig. 4). A SW-dipping thrust fault is interpreted in both the fieldwork and the satellite image. According to the stratigraphic correlation between the hanging-wall and footwall, the fault throw is inferred ~500 m. Therefore, the main thrust fault is a seismic-scale fault, corresponding to the fault  $F_1$  in Fig. 4. Based on the stratigraphic columns, the lithology changes from coarse sandstone to clay-rich fine sandstone towards the central fault  $F_1$ , in either the hanging-wall or the footwall. By integrating field dip measurements and satellite image interpretation, a high-resolution profile is constructed by using Busk method in the fault zone and kink-band algorithm in the further hanging-wall and footwall, which can be used to constrain the seismic interpretation. This high-resolution profile allows us to observe detailed structural features that are under seismic resolution. For example, the hanging-wall strata present downward steepening dips towards the fault  $F_1$ , whereas the footwall strata against the fault zone are overturned. These structural features observed in field also suggest that the layer thickness is not universally constant in the profile. Therefore, the well-established kink-band method (Suppe, 1983; Suppe and Medwedeff, 1990) is no longer applicable for the structural interpretation of the Lenghu5 fold-and-thrust belt. An appropriate deformation mechanism, potentially trishear algorithm, is necessary to understand the structural deformation happened in the Lenghu5 fold-and-thrust belt.

#### 4. Analogue Analysis by Trishear Models

The effects of trishear parameters on the geometry of trishear models have been evaluated by constructing a trishear parameter space (Pei et al., 2014). The trishear models in the parameter space focus on reverse faults with constant dip during deformation. The clusters of natural examples in the parameter space suggested p/s ratio of 2.0-2.5 and trishear apical angle of  $50^\circ$  for majority natural examples that have been investigated in previous studies (e.g., Allmendinger, 1998; Allmendinger et al., 2004; Cardozo, 2005; Cardozo and Aanonsen, 2009; Cardozo et al., 2005; Champion et al., 2001; Gold et al., 2006; Hardy and Ford, 1997; Lin et al., 2007). As the examples with different parameters in Fig. 7, monoclines are developed in front of the fault tip in the trishear models. Although these geometries are common to all examples, the specific resultant geometries vary significantly depending upon the specific parameters that are used. With a constant fault slip, the amplitude of the hanging wall uplift has a positive correlation with fault dip that is unaffected by p/s ratio or apical angle whereas the fault tip propagation is positively correlated with high p/s ratio and unaffected by apical angle or fault dip. Parameters of low fault dip, low p/s ratio and high apical angle result in a high magnitude of hanging wall thinning and footwall thickening, whereas parameters of low fault dip, low p/s ratio and high apical angle form a wide monocline. The monocline in front of the fault tip can be overturned with parameters of high fault dip, high p/s ratio and low apical angles. Moreover, the layers' thickness is not constant during deformation. For example, the hanging-wall strata are thinning and the footwall strata are thickening in all the trishear models. If the layers are cut by the propagating faults, 'dragging structures' are also observed in both hanging-wall and footwall adjacent to the faults. These features are also observed in the high-resolution fieldwork in the Lenghu5 fold-and-

thrust belt. The high accordance between the trishear models and the field observations indicate that trishear can be an appropriate approach to reveal the structural deformation happened to the Lenghu5 fold-and-thrust belt.

However, the simple trishear models cannot properly illustrate the geometry of hanging-wall and footwall in the Lenghu5 fold-and-thrust belt. For example, it is impossible to form an anticline in the hanging-wall with a constant-dipping reverse fault, and the minor folds presented in the footwall could not be formed with a single reverse fault in a structure (Fig. 6). The fault geometry is therefore more complex than the trishear models presented in Fig. 7. The factors that can increase the complexity of trishear models are, for example, fault-dip change and pre-existing faults (Allmendinger et al., 2004; Pei et al., 2014). Complex geometry is then formed by integrating these factors in trishear models. Here we consider trishear algorithm on curved reverse faults (i.e., fault-dip change) and multiple faults (i.e., pre-existing faults) for analogue analysis to predict the subsurface structures. In order to provide accurate geometric constraints on the structural deformation of the Lenghu5 fold-and-thrust belt, we investigate the structural geometry of the hanging-wall and footwall, individually.

We firstly apply trishear algorithm on curved reverse faults to test whether the Lenghu5 thrust fault is upward-steepening (p/s ratio of 2.0, apical angle of  $50^\circ$ , fault dip from  $10^\circ$  to  $70^\circ$ , Fig. 8b) or upward-shallowing (p/s ratio of 2.0, apical angle of  $50^\circ$ , fault dip from  $70^\circ$  to  $20^\circ$ , Fig. 8c) in subsurface. The upward-steepening and upward-shallowing reverse faults form very different hanging-wall geometries. The upward-steepening reverse fault forms an anticline in the hanging-wall, with a gentle backlimb and overturned forelimb (Fig. 8b), whereas the upward-shallowing reverse fault forms a monocline in the hanging-wall and the hanging-wall shows downward

steepening dips towards the triangle deformation zone (Fig. 8c). By comparing these two trishear models with the high-resolution surface data (e.g., dip distribution, Fig. 8a) in the Lenghu5 fold-and-thrust belt, the trishear model of upward-steepening reverse fault in Fig. 8b presents very similar hanging-wall geometry as observed in fieldwork. The upward-steepening trishear model can therefore provide good constraints on the hanging-wall geometry of the Lenghu5 fold-and-thrust belt. We then apply trishear algorithm on reverse faults with lower pre-existing faults to explain the footwall geometry of the Lenghu5 fold-and-thrust belt. The pre-existing faults could have either same or opposite thrusting direction with the upper reverse fault. For example, Fig. 9b depicts a trishear model of an upward-steepening reverse fault (p/s ratio of 2.0, apical angle of  $50^\circ$ , fault dip from  $70^\circ$  to  $80^\circ$ ) above two pre-existing faults (p/s ratio of 2.0, apical angle of  $50^\circ$ , fault dip from  $50^\circ$  to  $60^\circ$  and from  $30^\circ$  to  $40^\circ$ ) with same thrusting direction, whereas Fig. 9c presents a trishear model of an upward-steepening reverse fault (p/s ratio of 2.0, apical angle of  $50^\circ$ , fault dip from  $0^\circ$  to  $70^\circ$ ) above an opposite thrusting fault (p/s ratio of 2.0, apical angle of  $50^\circ$ , fault dip from  $20^\circ$  to  $40^\circ$ ). A pair of tight syncline and open anticline is developed in the footwall of the upper reverse fault in the trishear model of Fig. 9c, which shows similar footwall geometry with the minor structures observed in the footwall of the Lenghu5 fold-and-thrust belt (Fig. 9a). The dip distribution in the footwall also presents high accordance between the trishear model in Fig. 9c and the field observations in the Lenghu5 fold-and-thrust belt. Therefore, it indicates that an opposite-thrusting fault is pre-existed in lower subsurface beneath the upper reverse fault, which controls the structural geometry of the Lenghu5 fold-and-thrust belt.

## 5. Constraints of Trishear Models on Structural Geometry

According to the above analogue analysis by the trishear models, the Lenghu5 fold-and-thrust belt is probably controlled by an upward-steepening reverse fault (i.e., SW-dipping fault  $F_1$ ) above opposite-thrusting reverse faults in deeper subsurface (i.e., NE-dipping faults  $F_2$  and  $F_3$ ). In the seismic section (Fig. 4), the upward decreasing displacement of  $F_1$  suggests a trishear algorithm is applicable in this structure. Moreover, the reverse faults  $F_1$ ,  $F_2$  and  $F_3$  all present upward-steepening shapes, which is highly comparable with the complex trishear models (Fig. 8b, Fig. 9c). Therefore, we applied the trishear forward modelling to simulate the structural evolution of the Lenghu5 fold-and-thrust belt by allowing multiple curved faults in a single section. By employing the parameter space and strain quantification workflows (Pei et al., 2014), the parameters of the best-fit trishear model are determined, with an apical angle of  $50^\circ$  and p/s ratio of 2.0. The comparison between the fault slip (cutoffs B and B') and the fault tip propagation of  $F_2$  also suggests a trishear p/s ratio of  $\sim 2.0$ . In order to simulate the upward-steepening reverse faults  $F_1$  and  $F_2$ , we used the interpreted  $F_1$  and  $F_2$  as templates to define the stepwise values of upward-steepening fault dip angles (Fig. 10). The dip variation and slip along faults were measured to provide constraints on the forward trishear modelling to reveal the kinematic evolution of the Lenghu5 fold-and-thrust belt. For example, the fault  $F_1$  presents upward-steepening dip from  $5^\circ$ ,  $12^\circ$ ,  $20^\circ$ ,  $32^\circ$ ,  $45^\circ$  to  $60^\circ$ , with fault slip of 4.9 km, 1.3 km, 1.2 km, 1.1 km, 2.3 km and 1.1 km, respectively; whereas the fault  $F_2$  presents upward-steepening dip from  $25^\circ$ ,  $34^\circ$ ,  $44^\circ$  to  $55^\circ$ , with fault slip of 1.5 km, 0.8 km, 0.9 km and 0.8 km, respectively.

Fig. 11a-c depicts the progressive development of the Lenghu5 fold-and-thrust belt, based on the trishear forward modelling using 2DMove (Midland Valley). In Fig. 11a,

the normal fault  $F_2$  was developed to form a half-graben in the  $J_r$  strata followed by deposition of post-extension sequence from  $E_{1+2}$  to  $N_{2-1}$ ; in Fig. 11b, the stress field changed to be compressional which results in the inversion of  $F_2$  and the development of a small thrust fault  $F_3$ ; in Fig. 11c, an opposite thrust fault  $F_1$  was developed within  $E_3$  layer, forming the current hanging-wall anticline. After uplift and erosion to present, Fig. 11c presents a good match to the geometry of the Lenghu5 fold-and-thrust belt, both in surface dip distribution and subsurface structural feature. In order to make precise comparison between the trishear model and natural observation, we integrated seismic interpretation, field data & satellite image and trishear model to demonstrate the surface dip distribution and well logging (Fig. 12). Because of limited resolution of seismic reflection, the seismic interpretation (Fig. 12a) can only present a very general pattern of surface dip distribution, with poor reflection in vicinity of the thrust fault  $F_1$ . The detailed field dip measurements (Fig. 12b) compensate the limited resolution of seismic reflection, which allows precise comparison of surface dip distribution between natural structure and the trishear model. Although there is still geometric uncertainty between the trishear model and natural observation, the trishear model (Fig. 12c) presents more detailed surface dip distribution that is in good accordance with the seismic interpretation. The geometry of trishear model also presents proper match with the stratigraphic logging in Lengke1 well, i.e., repetition of  $N_1$  and  $E_3$  beneath the fault  $F_1$ .

The trishear forward models do not only reveal the detailed structural evolution of the Lenghu5 fold-and-thrust belt, but also present smaller scale structures that are under seismic resolution, which may help improve the understanding of detailed deformation happened in both the hanging-wall and footwall adjacent to the faults. For example, the dragging structures adjacent to  $F_1$  and  $F_2$  are not resolvable in

seismic section (Fig. 13a), and the minor syncline-anticline pair in the footwall are only observed in the trishear forward models (Fig. 13b). These detailed minor structures can constrain the fault and horizon interpretation in seismic section. For example, a) the detailed cross-cutting relationship between the horizons and faults could increase the accuracy of fault cutoffs interpretation in the seismic section, which is vital for determining fault displacement and propagation/slip ratio; b) the detailed intersecting relationship between the lower pre-existing fault  $F_2$  and the upper reverse fault  $F_1$  could also provide constraints on the fault tip interpretation in the seismic section. The trishear forward modelling, with the validation by high-resolution field data, can therefore be an effective technique for increasing the accuracy of seismic interpretation.

## 6. Discussion

### 6.1. Geometric constraints of trishear forward modelling

Balancing section restoration has been broadly employed to test the reliability of seismic interpretation. The conventional balancing restoration is working with a precondition that the layer thickness keeps constant during deformation or the horizon length keeps constant during deformation, for example, kink-band models. However, there are many structures in which the layer thickness and horizon length are changed during deformation, in both experimental analogue models (Bonini, 2007; Bose et al., 2009; Costa and Vendeville, 2002; Ellis et al., 2004; McQuarrie, 2004; Miller and Mitra, 2011) and natural geological structures (e.g., Allmendinger, 1998; Cristallini and Allmendinger, 2001; Cristallini et al., 2004; Erslev, 1991; Erslev and Mayborn, 1997; Erslev and Rogers, 1993; Pei et al., 2014; Pei et al., 2017). These structures present non-uniform dips in the same limb and inhomogeneous deformation adjacent to fault (zone). Consequently, as demonstrated by the Lenghu5

fold-and-thrust belt, the balancing section restoration following kink-band method is no longer applicable to verify the reliability of the seismic interpretation. In this situation, the trishear forward modelling could be taken into account to explain the complexity of the structural deformation, as the non-uniform deformation within the triangle zone in front of the fault tip allows the layer thickness and horizon length to change during deformation (Erslev, 1991; Hardy and Ford, 1997). By varying trishear parameters, a spectrum of trishear models with different geometries could be generated. The best-fit parameter combination can also be determined by employing the three-dimensional parameter space (Pei et al., 2014). The geometric spectrum and complexity of trishear models could also be increased by integrating fault-dip change, multiple faults and pre-existing faults in trishear forward modelling (Fig. 7). This allows the application of trishear algorithm to provide geometric constraints for the subsurface structural prediction. However, high complexity of the natural structures obviously increases the difficulty in finding an appropriate trishear solution. Therefore, some appropriate simplification of natural structures is necessary, as the first-order structures can provide initial geometric constraints to determine the best-fit trishear parameters. But this does not mean the small-scale structural features are completely neglected in the analogue analysis using trishear algorithm. The previously simplified structural complexity can be then reproduced in the trishear models to provide constraints for the structural interpretation in natural structures, e.g., the accurate prediction of fault cutoffs and fault tip (Fig. 13).

## **6.2. 'Ground truthing' by high-resolution field data**

Trishear forward modelling could be possibly used to predict subsurface structures with very different geometries. The strata dip changes and minor structural features in trishear models could also be employed to assist the subsurface prediction that

are under seismic resolution. The successful application of trishear forward modelling in the Lenghu5 fold-and-thrust belt has provided an effective workflow for subsurface structural interpretation with the assistance of trishear forward modelling. However, in the Lenghu5 fold-and-thrust belt, although there is good match of surface dip distribution, there is still discrepancy between the trishear model and natural observation. For example, the dip angle of  $N_1$  and  $N_{2-1}$  in the hanging-wall is higher than the field measurements in the hanging-wall; the  $N_1$  unit in the footwall presents significant thickening towards the fault  $F_1$ , which is not in strict accordance with the seismic interpretation. This may be attributed to the parameter setting during trishear forward modelling, particularly p/s ratio and apical angle (fault dip variation was well-constrained by the geometry of interpreted faults in seismic section). In this trishear forward modelling, the p/s ratio and apical angle were set with constant value of 2.0 and  $50^\circ$ , respectively. Although published case studies mostly used constant values for p/s ratio and apical angle for simplicity, geologists have realized that the trishear parameters may vary during the propagation of a fault. Therefore, high-resolution field data, such as stratigraphic logging and strata/fault dip measurements, can help improve accuracy of trishear models. Moreover, as there is a very wide spectrum of geometries in the trishear parameter space (Pei et al., 2014), it is vital to use stratigraphic logging and dip measurements to test the validity of the selected trishear models. Stratigraphic logging and dip measurement from multiple wells, apparently effective for structural validation, however, are unrealistic for a natural structure in many study areas. Therefore, high-resolution fieldwork, including regional stratigraphic logging and detailed dip measurements, can be employed as an effective 'ground truthing' tool to validate the trishear models. With the assistance of trishear forward modelling validated by high-resolution field data, the accuracy of

seismic interpretation can be significantly improved, particularly the interpretation of second-order structural features in the hanging-wall and footwall adjacent to the faults where the quality of seismic reflection is usually poor.

### **6.3. Effects of mechanical stratigraphy on trishear forward modelling**

This paper focuses on the geometric constraints of the trishear forward modelling on subsurface structural prediction, the trishear parameters  $p/s$  ratio and apical angle were therefore set as constant values (2.0 for  $p/s$  ratio and  $50^\circ$  for apical angle) without considering their variation during propagation of faults. However, we also realize that mechanical stratigraphy also plays an important control on geometry of resultant trishear models, because the trishear parameters can vary depending upon lithology and mechanical strength (e.g., Alonso and Teixell, 1992; Hardy and Finch, 2007; Hardy and Ford, 1997; Yang et al., 2014). In our study area, the hanging-wall and footwall of the Lenghu5 fold-and-thrust belt covers lithology ranging from conglomerates, coarse sandstones, medium sandstones, fine sandstones, siltstones and mudstones (see the stratigraphic columns in Fig. 6, Fig. 8a and Fig. 9a), which present fining direction towards the central fault zone of  $F_1$ . On the one hand, high competent rocks usually present higher  $p/s$  ratios and narrower apical angle than rocks with low competency (e.g., Allmendinger, 1998; Hardy and Ford, 1997; Pei et al., 2014; Welch et al., 2009a). Therefore, as demonstrated in the stratigraphic columns in our study area, the siltstone/mudstone-dominated stratigraphy adjacent to the fault  $F_1$  may present lower  $p/s$  ratio and wider apical angle than the sandstone-dominated lithology in the further hanging-wall and footwall. On the other hand, when it comes to interbedded rocks with different lithology, such as interbedded layers of sandstone and mudstone, the resultant structure may present high degree of geometric complexity with increasing mechanical heterogeneity. By employing

discrete-element technique (Finch et al., 2003, 2004; Hardy and Finch, 2007; Yang et al., 2014), stratigraphy with low to high mechanical heterogeneity has been investigated to understand their different structural deformation in response to contractional stress. Welch et al. (2009a; 2009b) also employed a quadrshear algorithm to study the complexity of folding deformation and fault architecture with different mechanical stratigraphy. Apparently, the Lenghu5 fold-and-thrust belt presents a certain level of stratigraphic heterogeneity in vertical direction, which may impact on the trishear forward models. However, it is still unrealistic to employ either discrete-element method or quadrshear algorithm to precisely simulate geometry and kinematics of natural examples with same level of structural complexity in the Lenghu5 fold-and-thrust belt. Field observation is, therefore, necessary to validate the application of trishear forward modelling. Both the Lenghu5 fold-and-thrust belt and the published mechanical models demonstrate the important influence of stratigraphy and strength on structural deformation, however, stratigraphic heterogeneity is likely to determine minor structural features that are superimposed upon the primary structural geometry. Therefore, when employing trishear algorithm for analogue analysis, caution should be given on the effects of mechanical stratigraphy, particularly at a scale that is comparable with the mechanical stratigraphy.

## **7. Conclusion**

This paper have presented a study using trishear forward modelling to constrain the structural deformation of natural structures. The following conclusions are drawn:

- 1) The best-fit trishear forward models for a natural structure could be identified by integrating high-resolution field data, e.g., stratigraphic logging, dip distribution and fault geometry. The best-fit trishear models could provide

geometric constraints on the subsurface faults and horizons picked in the seismic section with poor quality of reflection.

- 2) With the constraints provided by trishear forward models, the complexity of structural geometry that are under seismic resolution, e.g., high-angle dips, fault tip position, faults' intersecting relationship and horizon/fault cross-cutting relationship, can be reproduced to increase the accuracy of the seismic interpretation.

Trishear algorithm can be employed to improve the quality of seismic interpretation, particularly in seismic sections with poor reflection. However, the trishear models are not reliable until it has been properly validated by high-resolution field data.

### **Acknowledgements**

We would like to thank our colleagues Dr G. Lloyd, Dr J. Imber, Dr. A. Li, Dr. H. Lickorish and Prof R. J. Knipe for their helpful communications and suggestions contributing to this research. Thanks are also given to two anonymous reviewers and the editor Prof Michel Faure for their constructive suggestions that help improve quality of this manuscript. The support from Qinghai Oilfield of PetroChina, Rock Deformation Research (RDR) and Midland Valley is also highly appreciated. This work has been collaboratively supported by the National Natural Science Foundation of China (41502192, 41602143), Shandong Provincial Natural Science Foundation China (2014BSE28008), and Open Funding of the Key Laboratory of Tectonics and Petroleum Resources (NO.TPR-2016-02).

## Figure Captions

**Figure 1.** Fault-bend fold and fault-propagation fold based on kink band method (Suppe, 1983; Suppe and Medwedeff, 1990). (a) fault-bend fold; (b) fault-propagation fold. The kink-band models keep layer thickness consistent during structural deformation.

**Figure 2.** The conceptual trishear model and a natural example. (a) A natural trishear example presenting inconsistent layer thickness, from the Turner Valley anticline, foothills of the Canadian Rocky Mountains (modified from Allmendinger, 1998). (b) The conceptual model based on previous studies (e.g., Erslev, 1991; Hardy and Ford, 1997).

**Figure 3.** Structural geology of the Qaidam Basin. (a) Tectonic setting of the Qaidam Basin; (b) SRTM DEM overlaid by structural interpretation of the Qaidam Basin; (c) A basin-scale cross section constructed based on seismic reflection (modified from Yin et al., 2008b). Note: the south-verging detachment fault in deep subsurface in (c) was speculated and its existence is still under controversy.

**Figure 4.** The seismic section and structural interpretation present the primary structural geometry of the Lenghu5 fold-and-thrust belt. (a) Un-interpreted seismic section constrained by the Lengke1 well. (b) Structural interpretation. (c) Amplified seismic section depicting detailed reflection of growth strata in the N<sub>2-2</sub> strata.

**Figure 5.** The structural restoration using 'fault parallel flow' algorithm in 2D Move, Midland Valley. (a) Central portion of the seismic section showing fault cutoff points and potential cross-cutting relationship. (b) A partially restored section by moving the hanging-wall down the fault F<sub>1</sub>.

**Figure 6.** The high-resolution profile of the Lenghu5 fold-and-thrust belt, integrating satellite image interpretation (QuickBird image, spatial resolution of 1 m, from DigitalGlobal), stratigraphic logging data and field dip measurements. See the position of this profile in Fig. 4.

**Figure 7.** Geometry of trishear models of a single fault, with variable apical angle and fault dip. The fault dip does not change in individual section during deformation. Apparently, the simple trishear models with constant fault dip is not geometrically comparable with the Lenghu5 example.

**Figure 8.** Hanging-wall geometric constraints by trishear analogue models with changing fault dips in a section. (a) Hanging-wall portion of the Lenghu5 fold-and-thrust belt. Satellite image: QuickBird image, spatial resolution of 1 m, from DigitalGlobal. (b) An upward-steepening reverse fault. (c) An upward-shallowing reverse fault.

**Figure 9.** Footwall geometric constraints by trishear analogue models with pre-existing faults. (a) Hanging-wall portion of the Lenghu5 fold-and-thrust belt. Satellite image: QuickBird image, spatial resolution of 1 m, from DigitalGlobal. (b) A reverse fault above pre-existing faults. (c) A reverse fault above an opposite pre-existing fault.

**Figure 10.** Geometric constraints on forward trishear modelling, provided by the measurements (including fault dip and fault slip) of  $F_1$ ,  $F_2$  and  $F_3$  interpreted in the seismic section in Fig. 4b.

**Figure 11.** Structural evolution of the Lenghu5 fold-and-thrust belt revealed by trishear forward modelling. (a) Normal faulting in Jurassic extension and deposition of post-extension sequence from  $E_{1+2}$  to  $N_{2-1}$ . (b) Development of reversed thrust faults and folds in the early compression. (c) Development of the upper reverse fault in the late compression.

**Figure 12.** Integration of seismic interpretation, field observation & satellite image (QuickBird image, spatial resolution of 1 m, from DigitalGlobal) and trishear forward model in the Lenghu5 fold-thrust-belt. The comparison between the three sets of data demonstrates general accordance, however, the discrepancy also suggests that there may be uncertainty in parameter setting during the trishear forward modelling.

**Figure 13.** The constraints of structural complexity reproduced in trishear models on subsurface structural geometry in seismic section. (a) Seismic interpretation. (b) Trishear model. The accuracy of seismic interpretation can be highly increased with the geometric constraints on faults and horizons.

## References

- Allmendinger, R.W., 1998. Inverse and forward numerical modeling of trishear fault-propagation folds. *Tectonics* 17, 640-656.
- Allmendinger, R.W., Zapata, T., Manceda, R., Dzelalija, F., 2004. Trishear Kinematic Modeling of Structures, with Examples from the Neuquen Basin, Argentina. in K. R. McClay, eds., *Thrust tectonics and hydrocarbon systems: American Association of Petroleum Geologists Memoir* 82, 356-371.
- Alonso, J.L., Teixell, A., 1992. Forelimb Deformation in Some Natural Examples of Fault-Propagation Folds. in K. R. McClay, eds., *Thrust Tectonics*. Springer Netherlands, 175-180.
- Bonini, M., 2007. Deformation patterns and structural vergence in brittle-ductile thrust wedges: An additional analogue modelling perspective. *J Struct Geol* 29, 141-158.
- Bose, S., Mandal, N., Mukhopadhyay, D.K., Mishra, P., 2009. An unstable kinematic state of the Himalayan tectonic wedge: Evidence from experimental thrust-spacing patterns. *J Struct Geol* 31, 83-91.
- Burchfiel, B.C., Deng, Q., Molnar, P., Royden, L., Wang, Y., Zhang, P., Zhang, W., 1989. Intracrustal detachment within zones of continental deformation. *Geology* 17, 748-752.
- Cardozo, N., 2005. Trishear modeling of fold bedding data along a topographic profile. *J Struct Geol* 27, 495-502.
- Cardozo, N., Aanonsen, S., 2009. Optimized trishear inverse modeling. *J Struct Geol* 31, 546-560.

- Cardozo, N., Allmendinger, R.W., Morgan, J.K., 2005. Influence of mechanical stratigraphy and initial stress state on the formation of two fault propagation folds. *J Struct Geol* 27, 1954-1972.
- Champion, J., Mueller, K., Tate, A., Guccione, M., 2001. Geometry, numerical models and revised slip rate for the Reelfoot fault and trishear fault-propagation fold, New Madrid seismic zone. *Eng Geol* 62, 31-49.
- Cheng, X., Fu, S., Wang, H., Yu, X., Cheng, F., Liu, R., Du, W., Guo, Z., 2015. Geometry and kinematics of the Arlar strike-slip fault, SW Qaidam basin, China: New insights from 3-D seismic data. *J Asian Earth Sci* 98, 198-208.
- Cheng, X., Zhang, Q., Yu, X., Du, W., Liu, R., Bian, Q., Wang, Z., Zhang, T., Guo, Z., 2017. Strike-slip fault network of the Huangshi structure, SW Qaidam Basin: Insights from surface fractures and seismic data. *J Struct Geol* 94, 1-12.
- Costa, E., Vendeville, B.C., 2002. Experimental insights on the geometry and kinematics of fold-and-thrust belts above weak, viscous evaporitic decollement. *J Struct Geol* 24, 1729-1739.
- Cowgill, E., Yin, A., Feng, W.X., Qing, Z., 2000. Is the North Altyn fault part of a strike-slip duplex along the Altyn Tagh fault system? *Geology* 28, 255-258.
- Cowgill, E., Yin, A., Harrison, T.M., Wang, X.F., 2003. Reconstruction of the Altyn Tagh fault based on U-Pb geochronology: Role of back thrusts, mantle sutures, and heterogeneous crustal strength in forming the Tibetan Plateau. *J Geophys Res* 108, 2346.
- Cristallini, E.O., Allmendinger, R.W., 2001. Pseudo 3-D modeling of trishear fault-propagation folding. *J Struct Geol* 23, 1883-1899.

- Cristallini, E.O., Giambiagi, L., Allmendinger, R.W., 2004. True three-dimensional trishear: A kinematic model for strike-slip and oblique-slip deformation. *Geol Soc Am Bull* 116, 938-952.
- Cui, Z.Z., Li, Q.S., Wu, C.D., Yin, Z.X., Liu, H.B., 1995. The crustal and deep structure in Golmud-Ejin Qi GGT (in Chinese with English abstract). *Acta Geophysica Sinica* 38, 28-34.
- Dahlstrom, C.D.A., 1990. Geometric Constraints Derived from the Law of Conservation of Volume and Applied to Evolutionary Models for Detachment Folding. *American Association of Petroleum Geologists Bulletin* 74, 336-344.
- Deng, J., Wu, Z., Yang, J., Zhao, H., Liu, H., Lai, S., Di, Y., 1995. Crust-mantle petrological structure and deep processes along the Golmud-Ejin Qi geoscience section (in Chinese with English abstract). *Acta Geophysica Sinica* 38, 144-157.
- Ellis, S., Schreurs, G., Panien, M., 2004. Comparisons between analogue and numerical models of thrust wedge development. *J Struct Geol* 26, 1659-1675.
- Erslev, E.A., 1991. Trishear Fault-Propagation Folding. *Geology* 19, 617-620.
- Erslev, E.A., Mayborn, K.R., 1997. Multiple geometries and modes of fault-propagation folding in the Canadian thrust belt. *J Struct Geol* 19, 321-335.
- Erslev, E.A., Rogers, J.L., 1993. Basement-Cover Geometry of Laramide Fault-Propagation Folds. *Geological Society of America Special papers* 280, 125-146.
- Finch, E., Hardy, S., Gawthorpe, R., 2003. Discrete element modelling of contractional fault-propagation folding above rigid basement fault blocks. *J Struct Geol* 25, 515-528.
- Finch, E., Hardy, S., Gawthorpe, R., 2004. Discrete-element modelling of extensional fault-propagation folding above rigid basement fault blocks. *Basin Res* 16, 467-488.

- Gao, R., Chen, X., Ding, Q., 1995. Preliminary geodynamic model of Goldmud-Ejin Qi geoscience transect (in Chinese with English abstract). *Acta Geophysica Sinica* 38, 14-27.
- Gold, R.D., Cowgill, E., Wang, X.F., Chen, X.H., 2006. Application of trishear fault-propagation folding to active reverse faults: examples from the Dalong Fault, Gansu Province, NW China. *J Struct Geol* 28, 200-219.
- Hardy, S., Finch, E., 2007. Mechanical stratigraphy and the transition from trishear to kink-band fault-propagation fold forms above blind basement thrust faults: A discrete-element study. *Mar Petrol Geol* 24, 75-90.
- Hardy, S., Ford, M., 1997. Numerical modeling of trishear fault propagation folding. *Tectonics* 16, 841-854.
- Jamison, W.R., 1987. Geometric Analysis of Fold Development in Overthrust Terranes. *J Struct Geol* 9, 207-219.
- Jolivet, M., Brunel, M., Seward, D., Xu, Z., Yang, J., Malavieille, J., Roger, F., Leyreloup, A., Arnaud, N., Wu, C., 2003. Neogene extension and volcanism in the Kunlun Fault Zone, northern Tibet: New constraints on the age of the Kunlun Fault. *Tectonics* 22, 1-23.
- Lin, M.L., Wang, C.P., Chen, W.S., Yang, C.N., Jeng, F.S., 2007. Inference of trishear-faulting processes from deformed pregrowth and growth strata. *J Struct Geol* 29, 1267-1280.
- Liu, D.L., Fang, X.M., Gao, J.P., Wang, Y.D., Zhang, W.L., Miao, Y.F., Liu, Y.Q., Zhang, Y.Z., 2009. Cenozoic Stratigraphy Deformation History in the Central and Eastern of Qaidam Basin by the Balance Section Restoration and its Implication. *Acta Geol Sin-Engl* 83, 359-371.

- Mao, L., Xiao, A., Zhang, H., Wu, Z., Wang, L., Shen, Y., Wu, L., 2016. Structural deformation pattern within the NW Qaidam Basin in the Cenozoic era and its tectonic implications. *Tectonophysics* 687, 78-93.
- McQuarrie, N., 2004. Crustal scale geometry of the Zagros fold-thrust belt, Iran. *J Struct Geol* 26, 519-535.
- Medwedeff, D.A., Suppe, J., 1997. Multibend fault-bend folding. *J Struct Geol* 19, 279-292.
- Meyer, B., Tapponnier, P., Bourjot, L., Metivier, F., Gaudemer, Y., Peltzer, G., Shunmin, G., Zhitai, C., 1998. Crustal thickening in Gansu-Qinghai, lithospheric mantle subduction, and oblique, strike-slip controlled growth of the Tibet plateau. *Geophys J Int* 135, 1-47.
- Miller, J.F., Mitra, S., 2011. Deformation and secondary faulting associated with basement-involved compressional and extensional structures. *American Association of Petroleum Geologists Bulletin* 95, 675-689.
- Mitra, S., 1990. Fault-Propagation Folds: Geometry, Kinematic Evolution, and Hydrocarbon Traps (1). *American Association of Petroleum Geologists Bulletin* 74, 921-945.
- Mitra, S., 2003. A unified kinematic model for the evolution of detachment folds. *J Struct Geol* 25, 1659-1673.
- Molnar, P., Tapponnier, P., 1975. Cenozoic Tectonics of Asia - Effects of a Continental Collision. *Science* 189, 419-426.
- Pei, Y., Paton, D.A., Knipe, R.J., 2014. Defining a 3-dimensional trishear parameter space to understand the temporal evolution of fault propagation folds. *J Struct Geol* 66, 284-297.

- Pei, Y., Paton, D.A., Knipe, R.J., Wu, K., 2017. Examining fault architecture and strain distribution using geospatial and geomechanical modelling: An example from the Qaidam basin, NE Tibet. *Mar Petrol Geol* 84, 1-17.
- Poblet, J., McClay, K., 1996. Geometry and kinematics of single-layer detachment folds. *American Association of Petroleum Geologists Bulletin* 80, 1085-1109.
- Suppe, J., 1983. Geometry and Kinematics of Fault-Bend Folding. *Am J Sci* 283, 684-721.
- Suppe, J., Medwedeff, D.A., 1990. Geometry and Kinematics of Fault-Propagation Folding. *Eclogae Geol Helv* 83, 409-454.
- Tapponnier, P., Meyer, B., Avouac, J.P., Peltzer, G., Gaudemer, Y., Guo, S.M., Xiang, H.F., Yin, K.L., Chen, Z.T., Cai, S.H., Dai, H.G., 1990. Active Thrusting and Folding in the Qilian-Shan, and Decoupling between Upper Crust and Mantle in Northeastern Tibet. *Earth Planet Sc Lett* 97, 382-403.
- Tavani, S., Storti, F., Salvini, F., 2005. Rounding hinges to fault-bend folding: geometric and kinematic implications. *J Struct Geol* 27, 3-22.
- Wang, E.C., Burchfiel, B.C., 2004. Late cenozoic right-lateral movement along the Wenquan fault and associated deformation: Implications for the kinematic history of the Qaidam Basin Northeastern Tibetan Plateau. *Int Geol Rev* 46, 861-879.
- Wei, Y., Xiao, A., Wu, L., Mao, L., Zhao, H., Shen, Y., Wang, L., 2016. Temporal and spatial patterns of Cenozoic deformation across the Qaidam Basin, Northern Tibetan Plateau. *Terra Nova* 28, 409-418.
- Welch, M.J., Davies, R.K., Knipe, R.J., Tueckmantel, C., 2009a. A dynamic model for fault nucleation and propagation in a mechanically layered section. *Tectonophysics* 474, 473-492.

- Welch, M.J., Knipe, R.J., Souque, C., Davies, R.K., 2009b. A Quadshear kinematic model for folding and clay smear development in fault zones. *Tectonophysics* 471, 186-202.
- Wu, L., Xiao, A., Ma, D., Li, H., Xu, B., Shen, Y., Mao, L., 2014. Cenozoic fault systems in southwest Qaidam Basin, northeastern Tibetan Plateau: Geometry, temporal development, and significance for hydrocarbon accumulation. *Aapg Bull* 98, 1213-1234.
- Xia, W.C., Zhang, N., Yuan, X.P., Fan, L.S., Zhang, B.S., 2001. Cenozoic Qaidam basin, China: A stronger tectonic inversed, extensional rifted basin. *American Association of Petroleum Geologists Bulletin* 85, 715-736.
- Yang, Y.-R., Hu, J.-C., Lin, M.-L., 2014. Evolution of coseismic fault-related folds induced by the Chi–Chi earthquake: A case study of the Wufeng site, Central Taiwan by using 2D distinct element modeling. *J Asian Earth Sci* 79, Part A, 130-143.
- Yin, A., Dang, Y., Zhang, M., McRivette, M.W., Burgess, W.P., Chen, X., 2007. Cenozoic tectonic evolution of Qaidam basin and its surrounding regions (part 2): Wedge tectonics in southern Qaidam basin and the Eastern Kunlun Range. *Geological Society of America Special Papers* 433, 369-390.
- Yin, A., Dang, Y.Q., Wang, L.C., Jiang, W.M., Zhou, S.P., Chen, X.H., Gehrels, G.E., McRivette, M.W., 2008a. Cenozoic tectonic evolution of Qaidam basin and its surrounding regions (Part 1): The southern Qilian Shan-Nan Shan thrust belt and northern Qaidam basin. *Geol Soc Am Bull* 120, 813-846.
- Yin, A., Dang, Y.Q., Zhang, M., Chen, X.H., McRivette, M.W., 2008b. Cenozoic tectonic evolution of the Qaidam basin and its surrounding regions (Part 3): Structural geology, sedimentation, and regional tectonic reconstruction. *Geol Soc Am Bull* 120, 847-876.

Yin, A., Harrison, T.M., 2000. Geologic Evolution of the Himalayan-Tibetan Orogen. *Earth and Planetary Sciences* 28, 211-280.

Yu, X., Fu, S., Guan, S., Huang, B., Cheng, F., Cheng, X., Zhang, T., Guo, Z., 2014. Paleomagnetism of Eocene and Miocene sediments from the Qaidam basin: Implication for no integral rotation since the Eocene and a rigid Qaidam block. *Geochemistry Geophysics Geosystems* 15, 2109-2127.

Zhou, J.X., Xu, F.Y., Wang, T.C., Cao, A.F., Yin, C.M., 2006. Cenozoic deformation history of the Qaidam Basin, NW China: Results from cross-section restoration and implications for Qinghai-Tibet Plateau tectonics. *Earth Planet Sc Lett* 243, 195-210.

Zhu, L.D., Wang, C.S., Zheng, H.B., Xiang, F., Yi, H.S., Liu, D.Z., 2006. Tectonic and sedimentary evolution of basins in the northeast of Qinghai-Tibet Plateau and their implication for the northward growth of the plateau. *Palaeogeography, Palaeoclimatology, Palaeoecology* 241, 49-60.

Figure 1

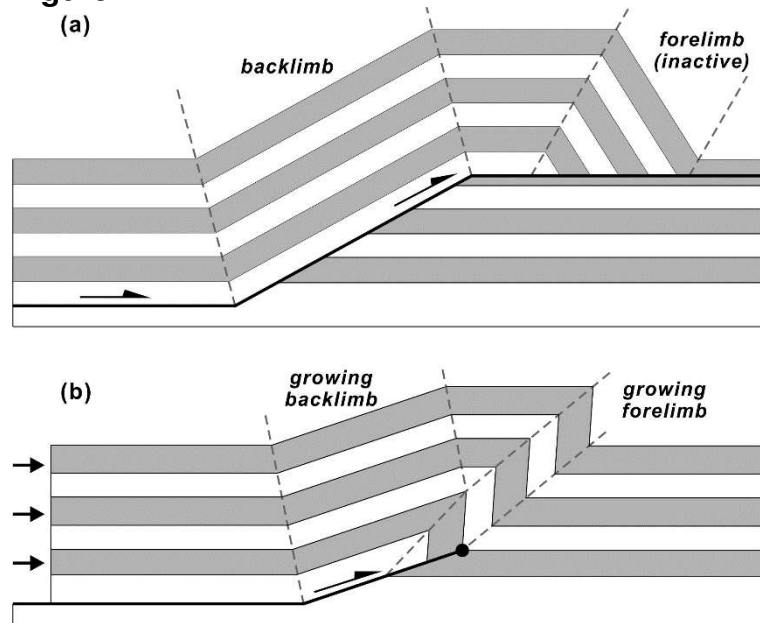
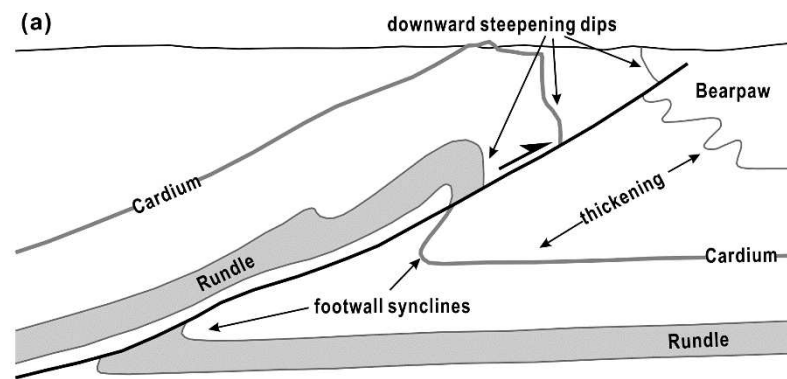


Figure 2



(b)

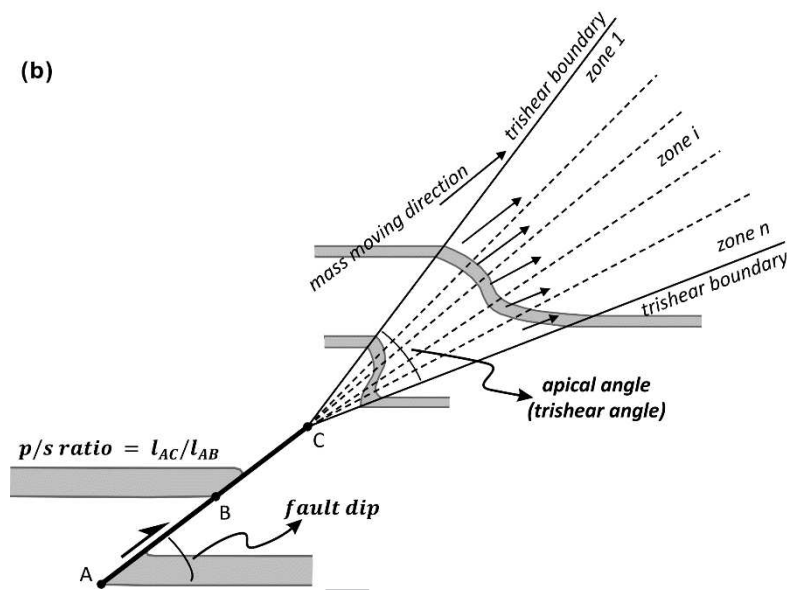


Figure 3

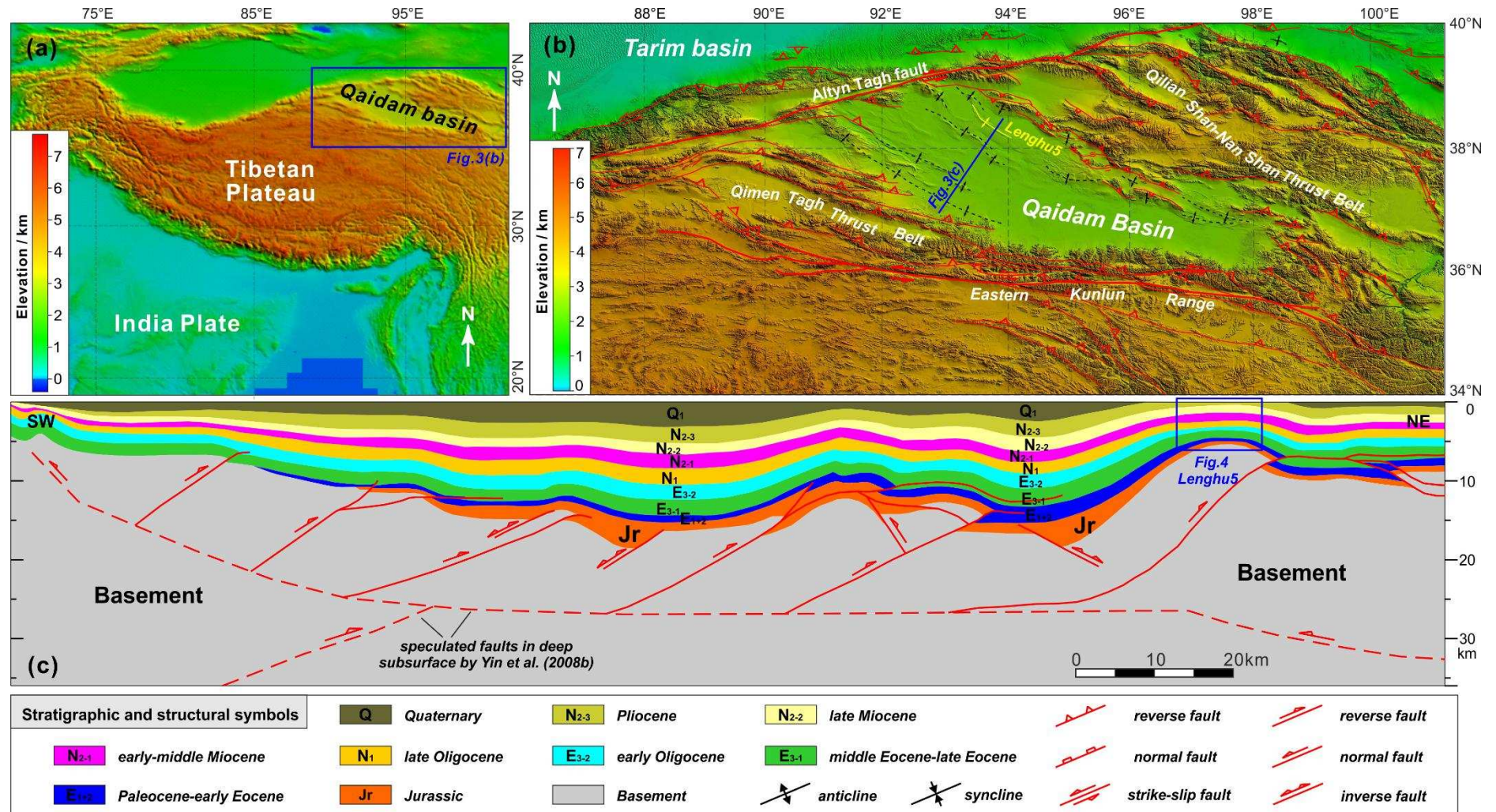


Figure 4

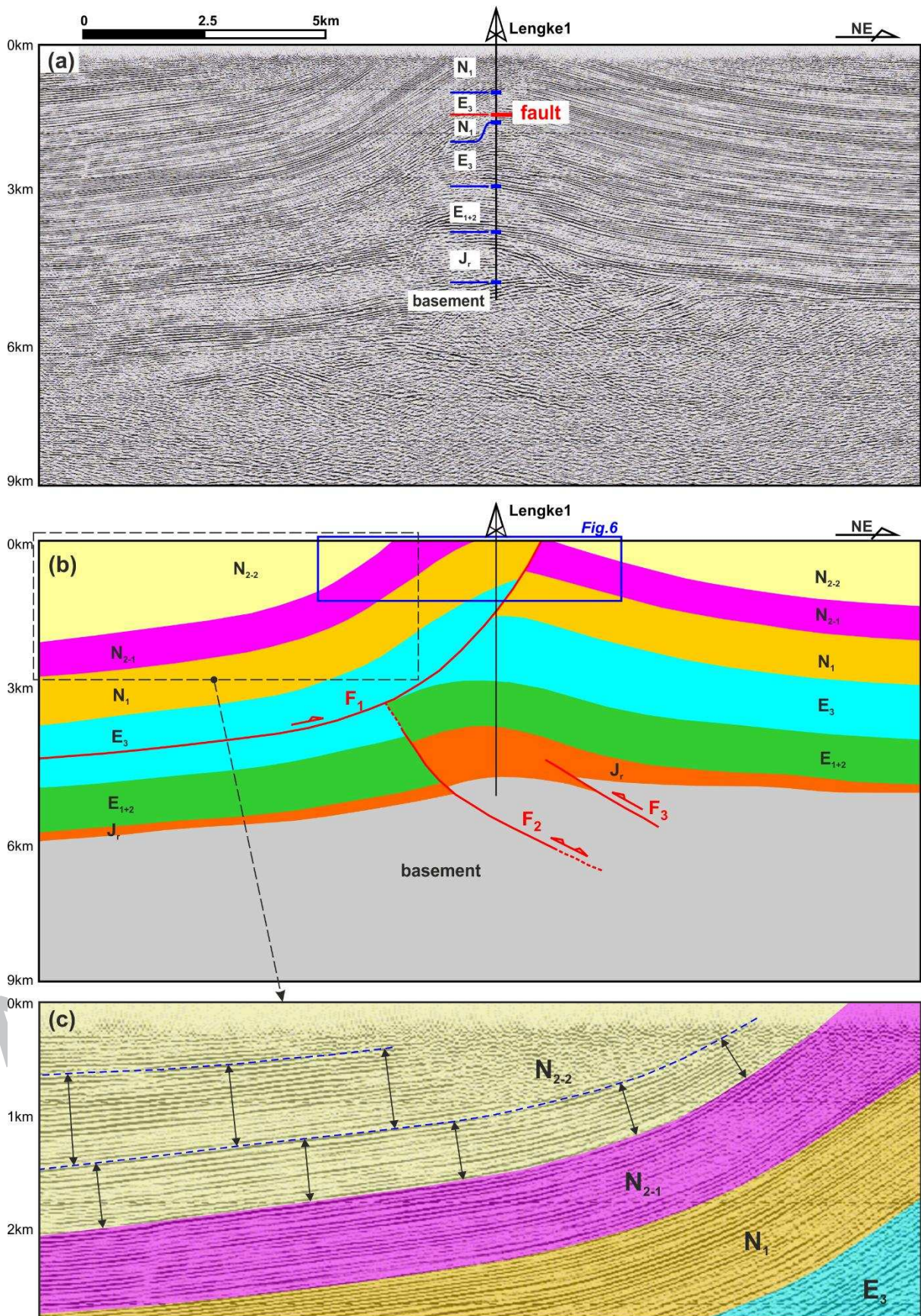


Figure 5

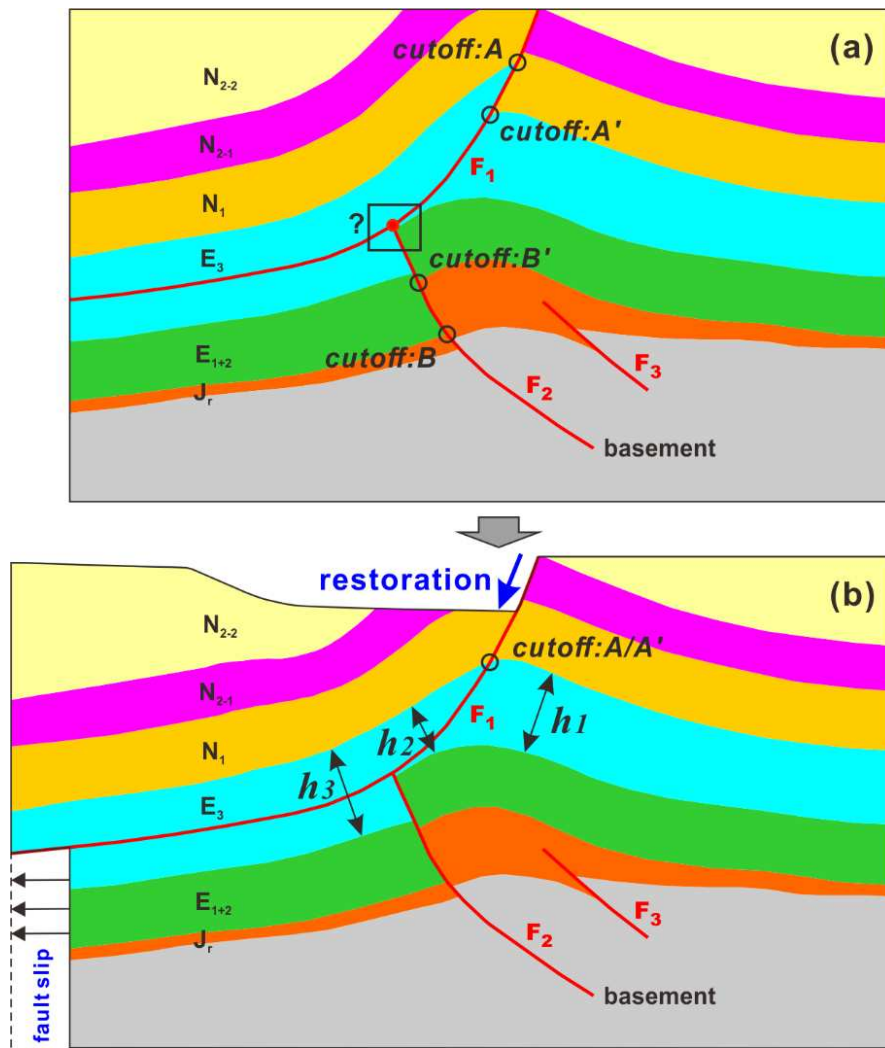


Figure 6

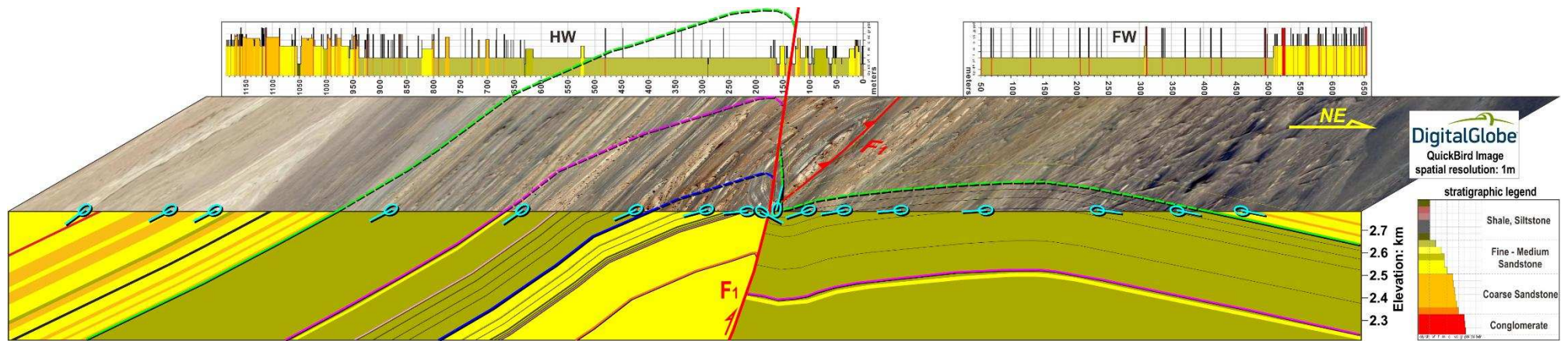


Figure 7

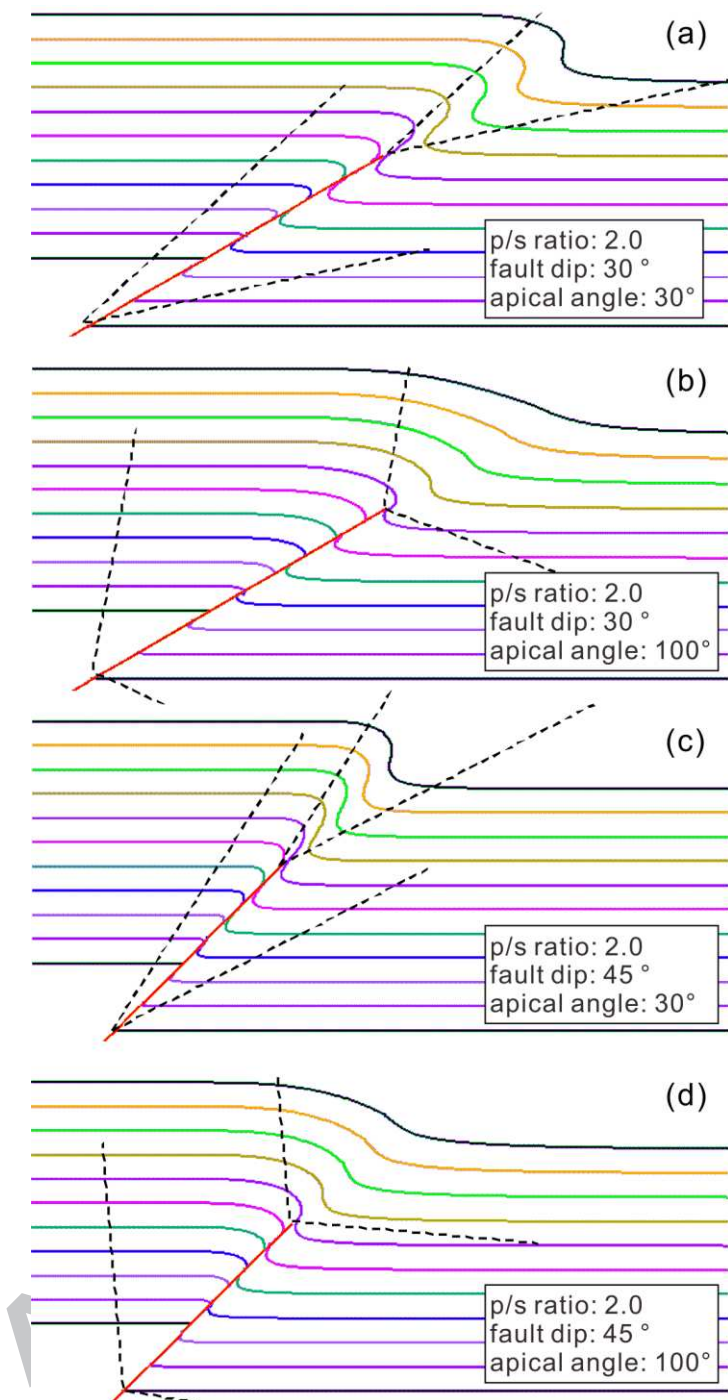


Figure 8

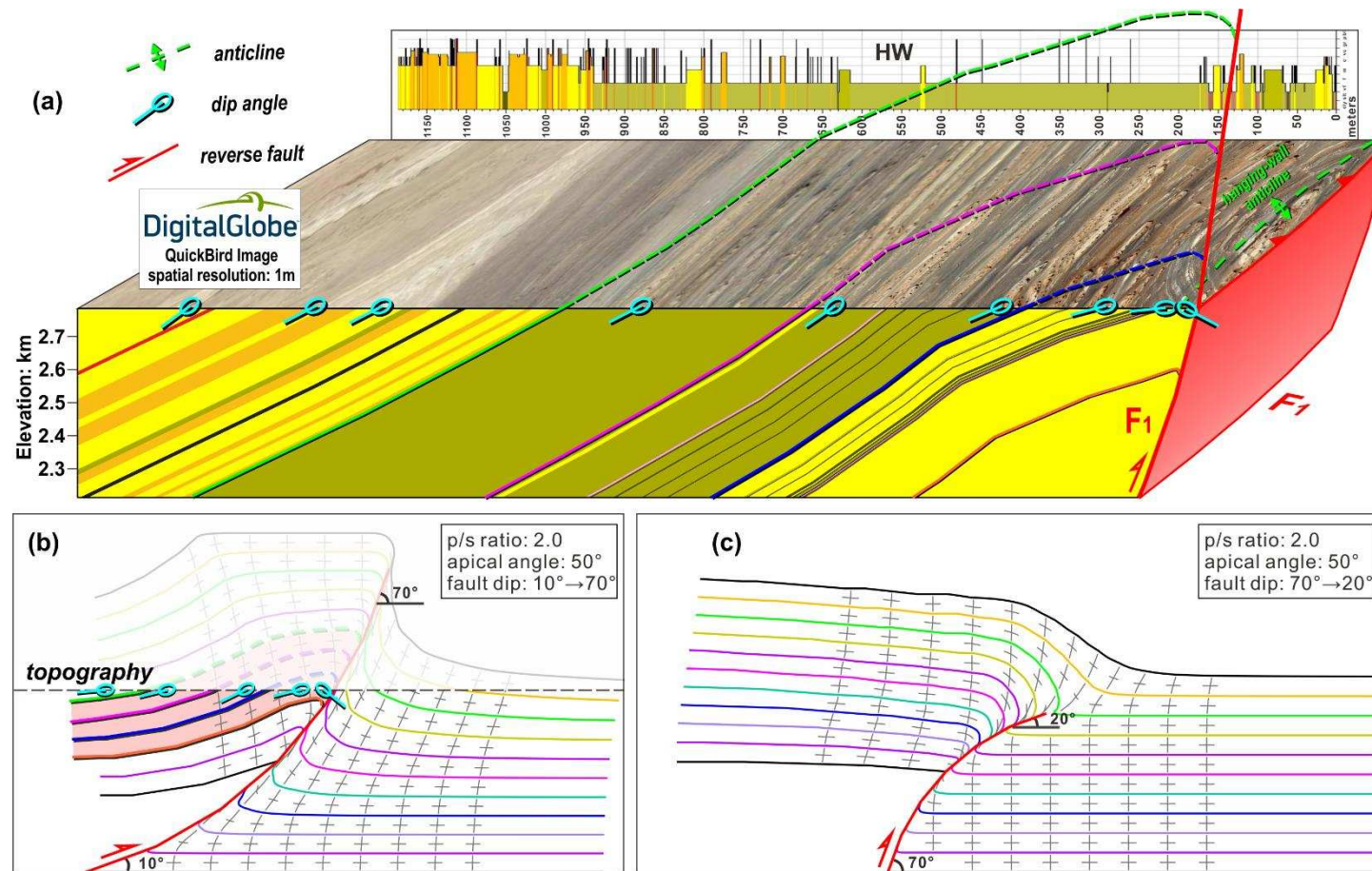


Figure 9

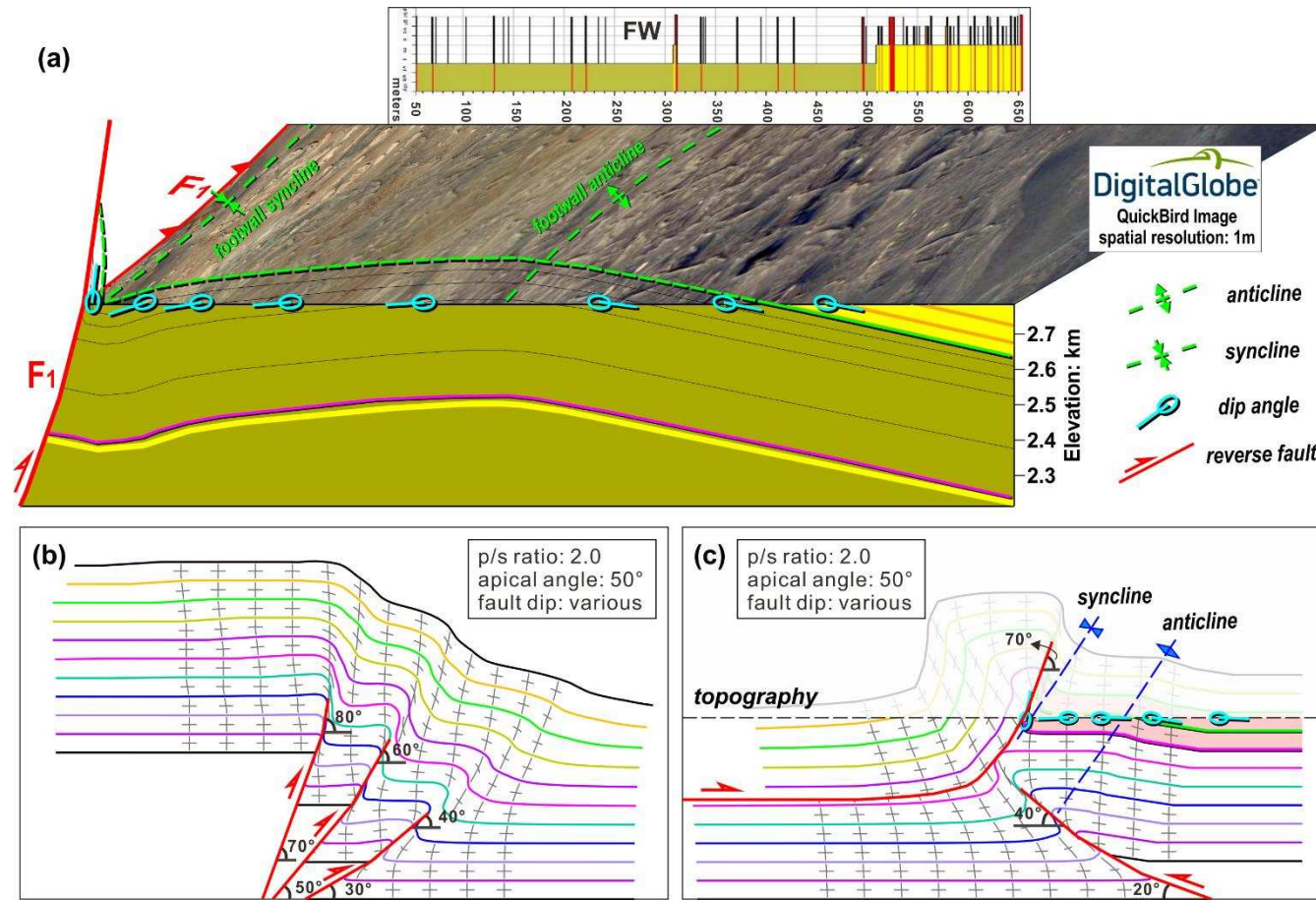


Figure 10

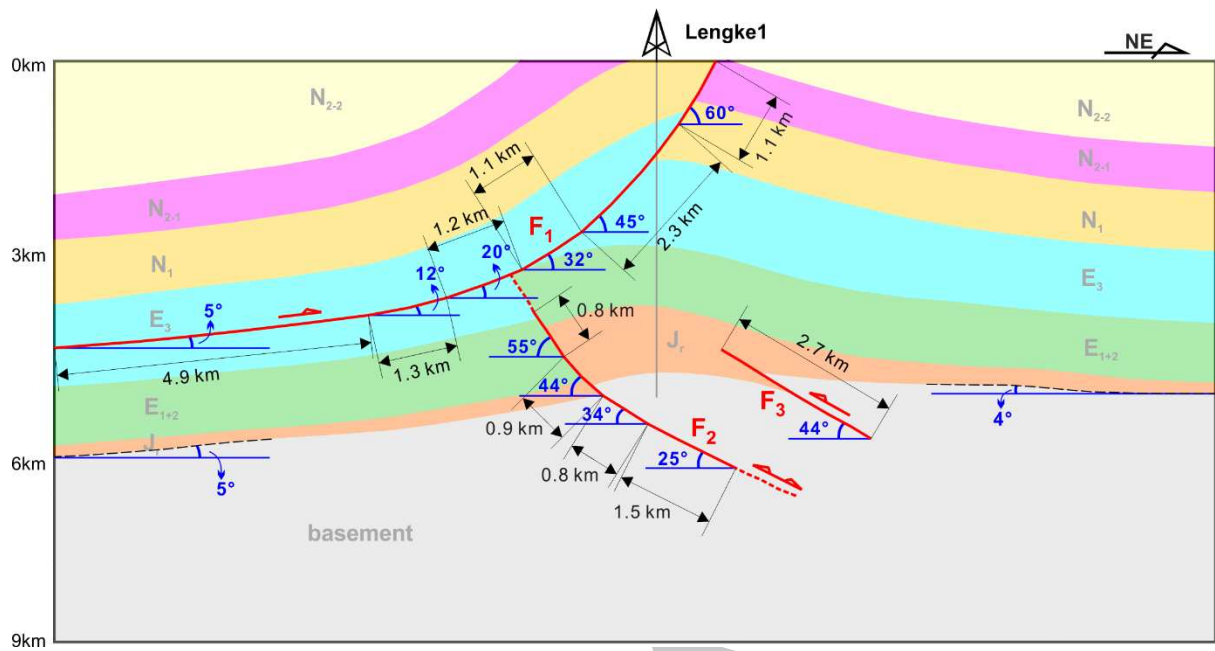


Figure 11

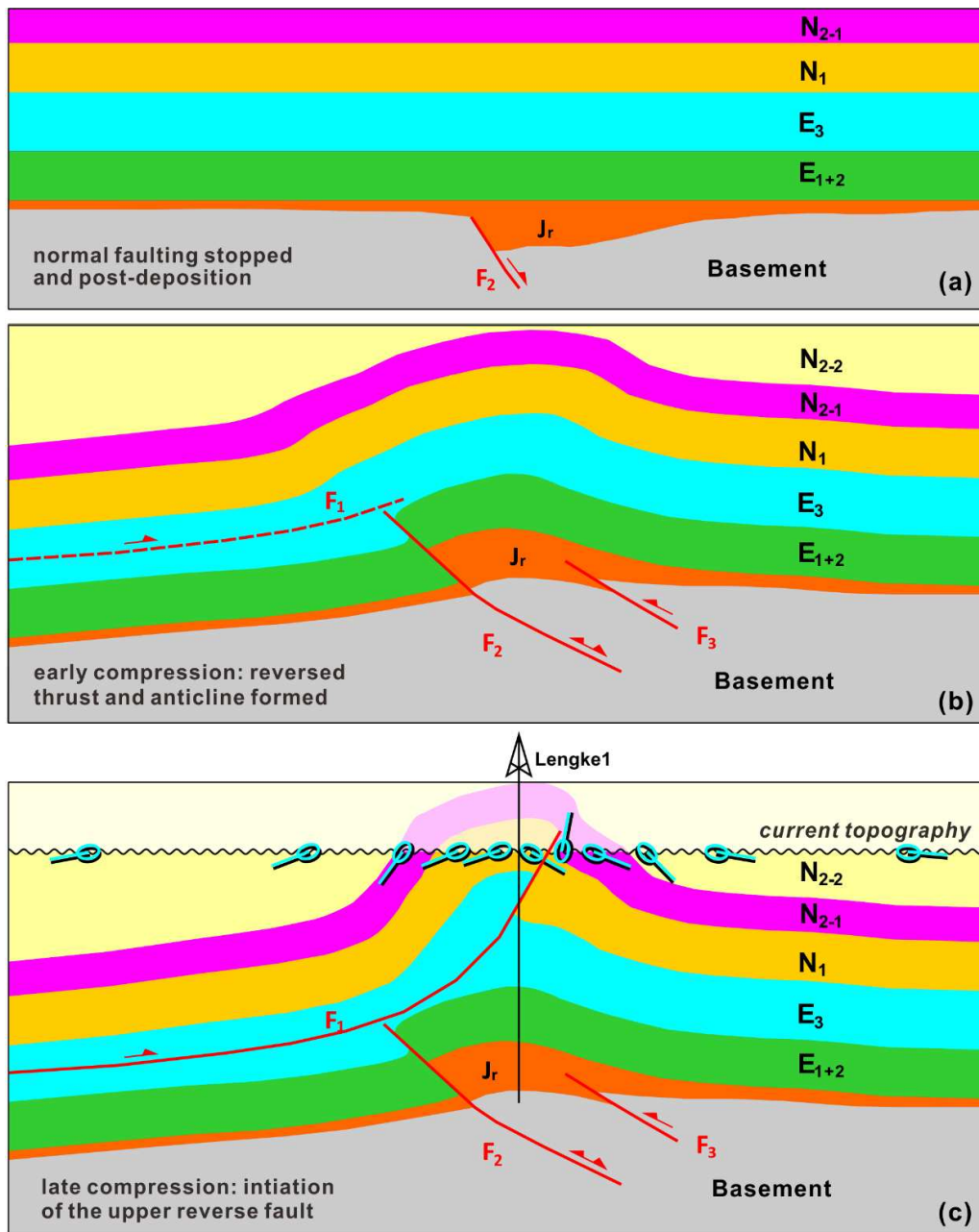


Figure 12

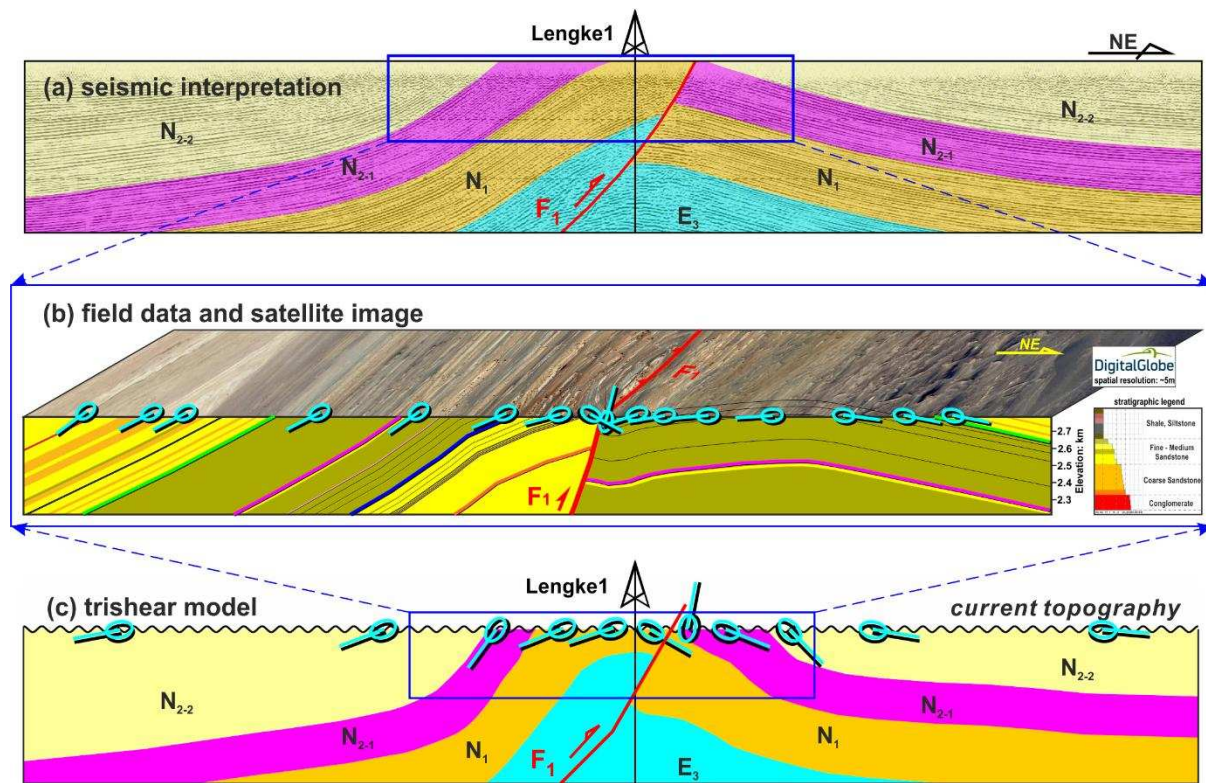
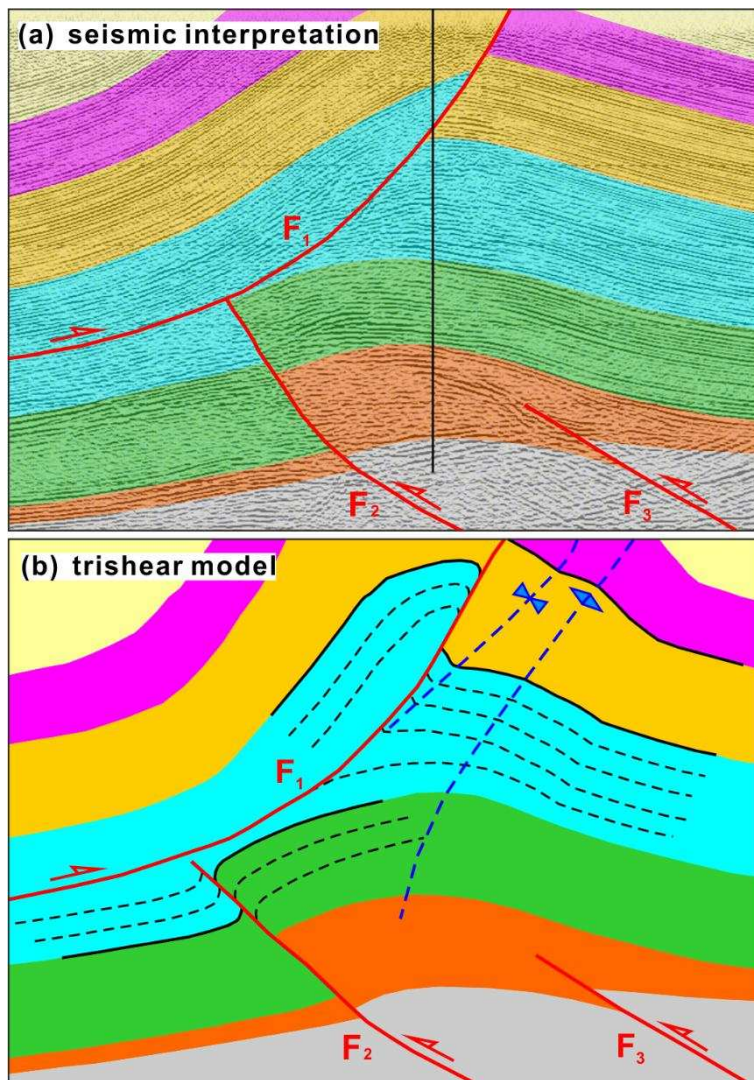
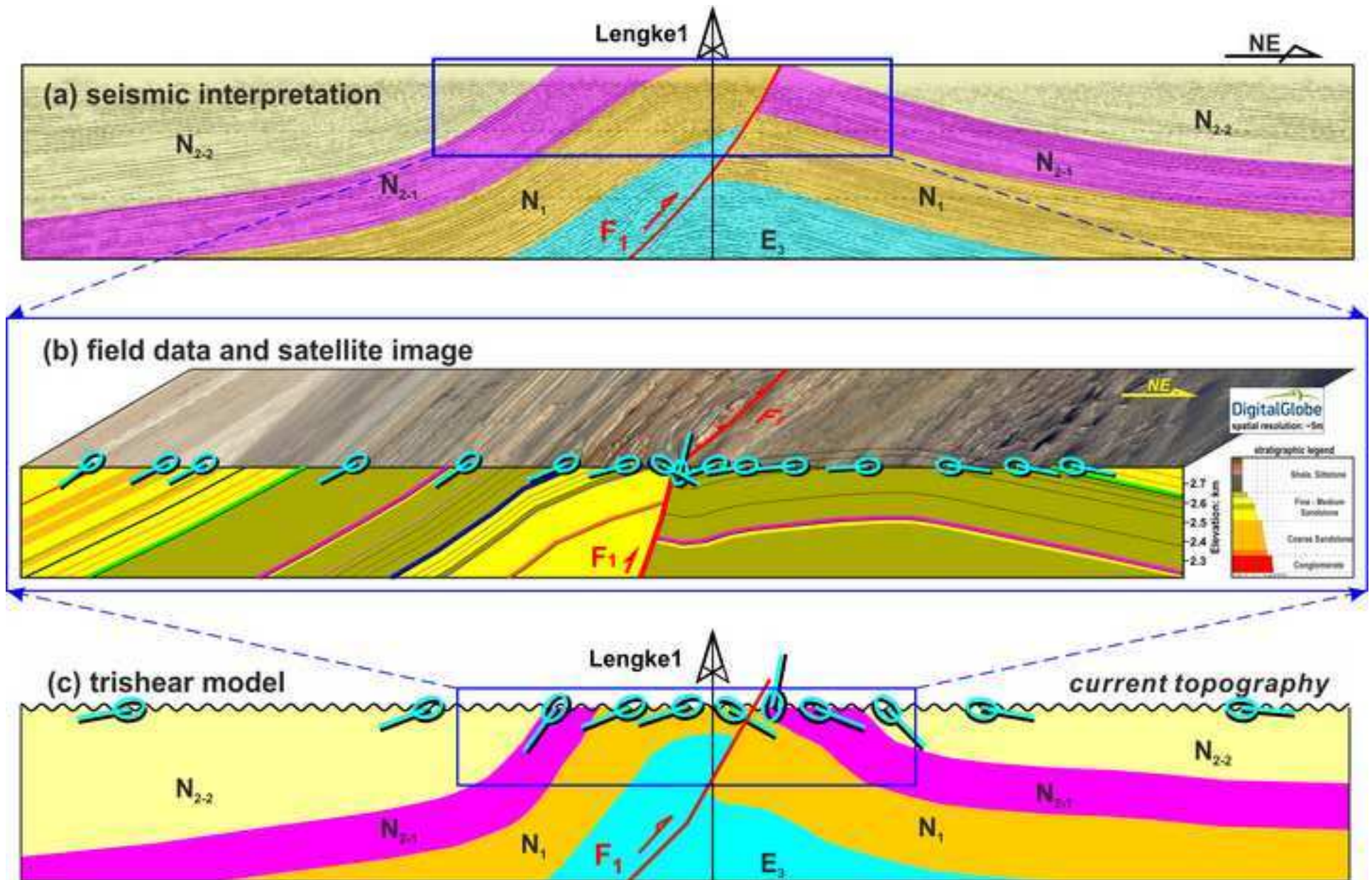


Figure 13





**Highlights**

- Trishear algorithm can generate a wide spectrum of structural geometry.
- High-resolution field data can help determine the best-fit model for natural example.
- Structures under seismic resolution can be built by trishear forward modelling.
- Trishear model provides geometric constraints to predict subsurface structures.

ACCEPTED MANUSCRIPT